

Supporting Information

Uniquely fabricated Cu(II)-metallacycle as reusable highly sensitive dual-channel and practically functional metalloceptor for Fe³⁺ and Ca²⁺ ions: An inorganic site of cation detection

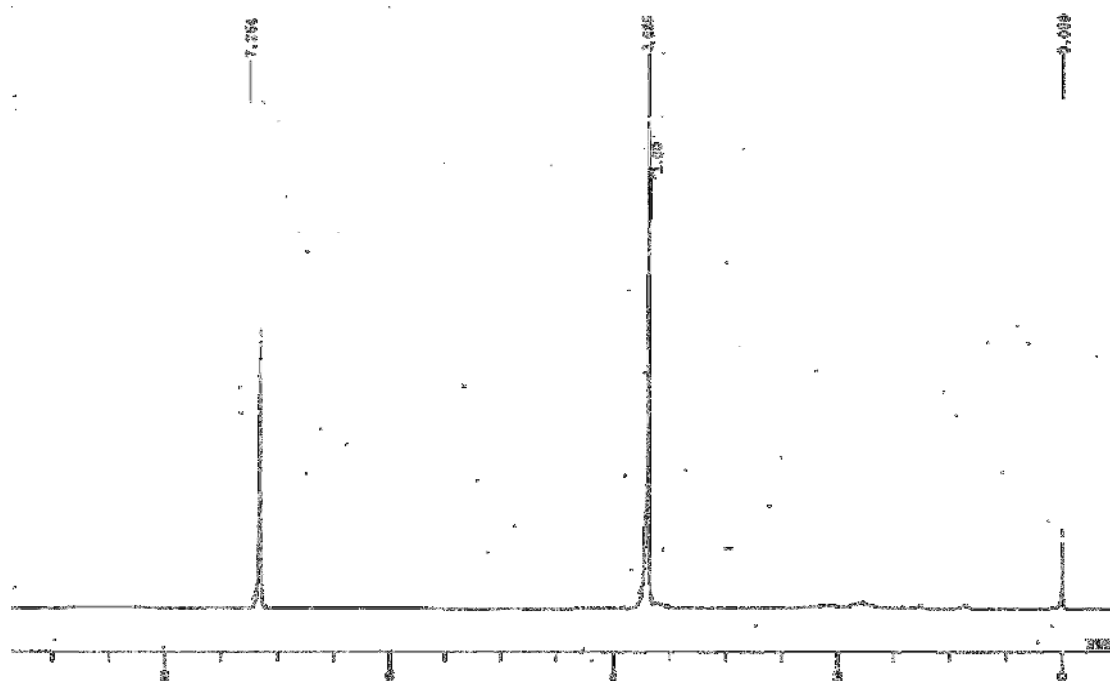
Neha Thakur, Mrituanjay D. Pandey* and Rampal Pandey*

Department of Chemistry, Dr. Harisingh Gour Central University, Sagar (MP), India

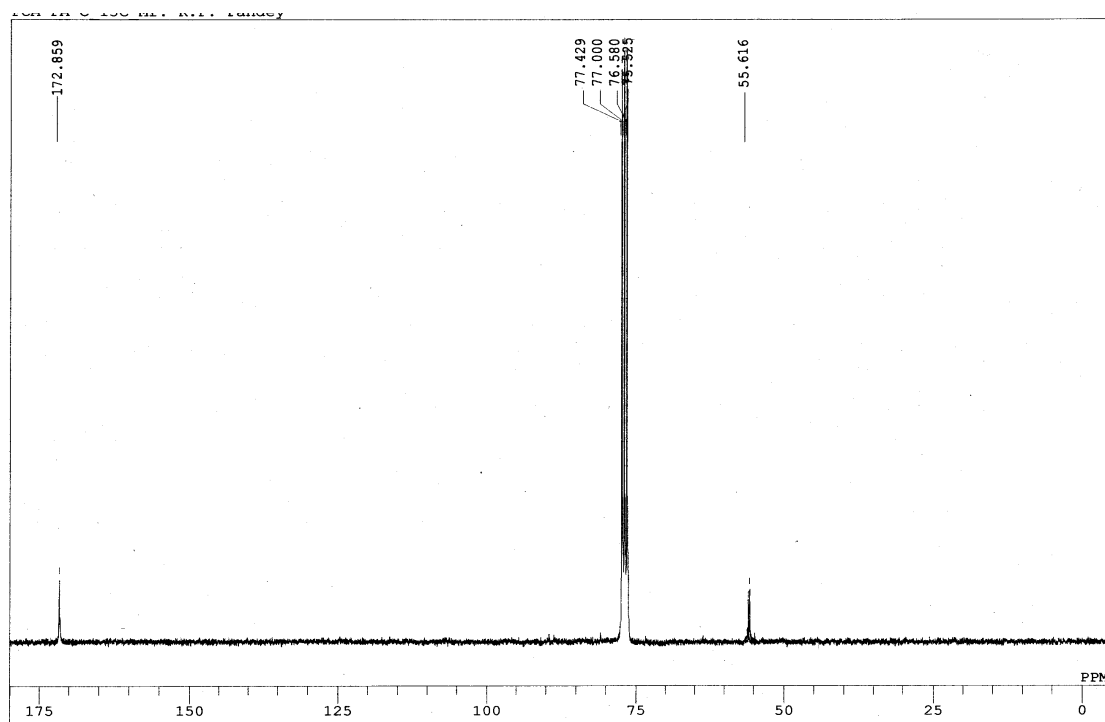
Contents:

Fig. S1&S2 ¹ H & ¹³ C NMR spectra of 1 and 2	S2-S3
Fig. S3 ESI-MS spectra of (a) 1 , (b) 2 and (c) 4	S4
Scheme S1&S2 Plausible mechanism for formation of 1 and 3 or 4	S5-S6
Fig. S4-S6 Crystal structures, discussions and weak interactions in 1-4	S6-S11
Fig. S7 UV/vis and Fluorescence discussion and spectra of 1-4	S11-S12
Fig. S8 Fluorescence spectra of 4 at various pH and dilution to check aggregation.....	S13
Fig. S9 UV/vis titration plot for 4 with Fe ³⁺ ion.....	S13
Fig. S10 Stern-Volmer plot for 4 and Fe ³⁺ ion.....	S14
Fig. S11 Jobs plot analysis for 4 +Fe ³⁺ ion 4 +Ca ²⁺ ion.....	S14
Fig. S12 Benesi-Hildebrand plot for 4 +Fe ³⁺ ion 4 +Ca ²⁺ ion.....	S15
Fig. S13 Interference studies both for Fe ³⁺ and Ca ²⁺ ions.....	S15-S16
Fig. S14&S15 Fluorescence sensitivity of 4 for Fe ³⁺ and Ca ²⁺ ions.....	S16-S17
Fig. S16 Reusability of 4 towards Fe ³⁺ and Ca ²⁺ ions using EDTA.....	S17-S18
Fig. S17 Discussion and structure of binding mode of 4 with Fe ³⁺ and Ca ²⁺ ions.....	S18-S19
Fig. S18 Fluorescence spectra of 3 in presence of various metal ions.....	S19
Fig. S19 CV discussion and plots of 1-4	S20-S21
Fig. S20 Electrochemical changes in 4 in presence of various metal ions.....	S12
Fig. S21 Electrochemical Hg ²⁺ interference with 4 +Fe ³⁺ and 4 +Ca ²⁺ complexes.	S12
Fig. S22 ESI-MS spectra of 4 +Fe ³⁺ ion 4 +Ca ²⁺ complexes.....	S23-S24
Fig. S23 Fluorescence quenching of 4 in real water samples.....	S25
TableS1 and References	S26-27

Supporting Information



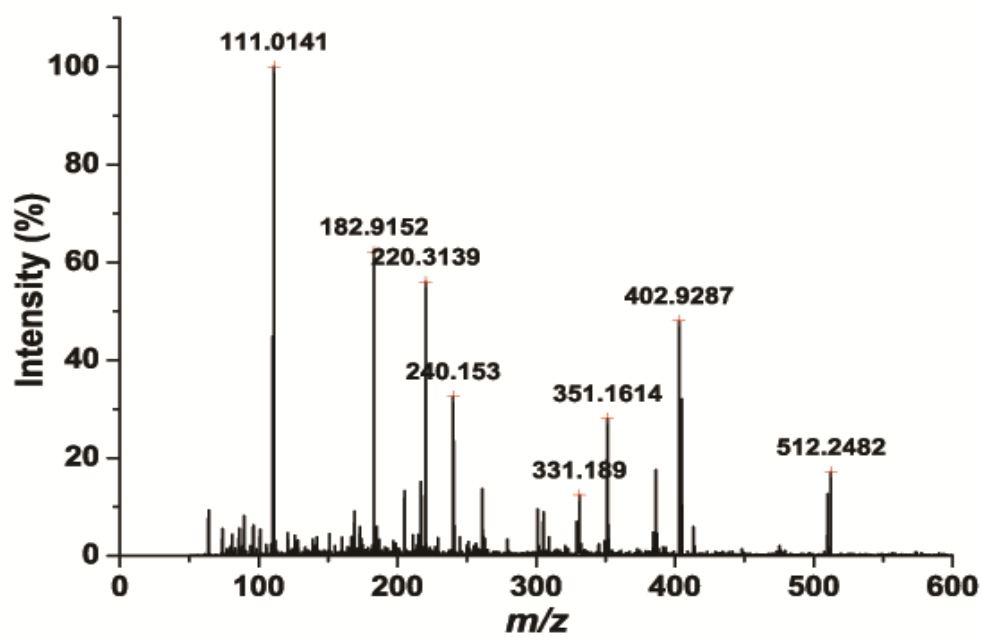
(a)



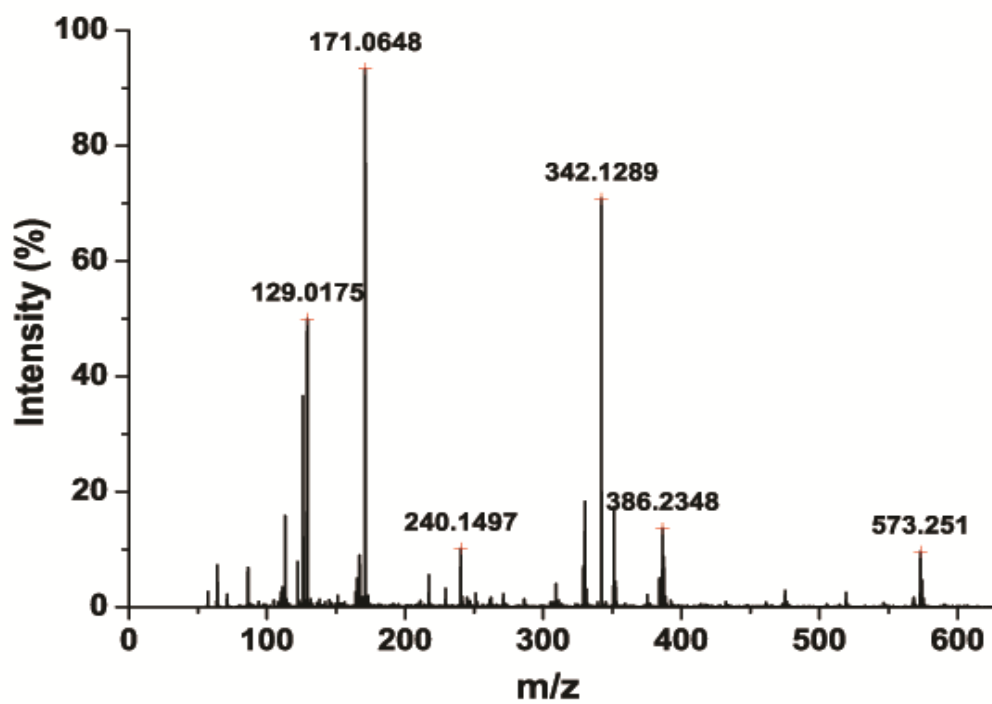
(b)

Fig. S2 ¹H & ¹³C NMR spectra of 2

Supporting Information

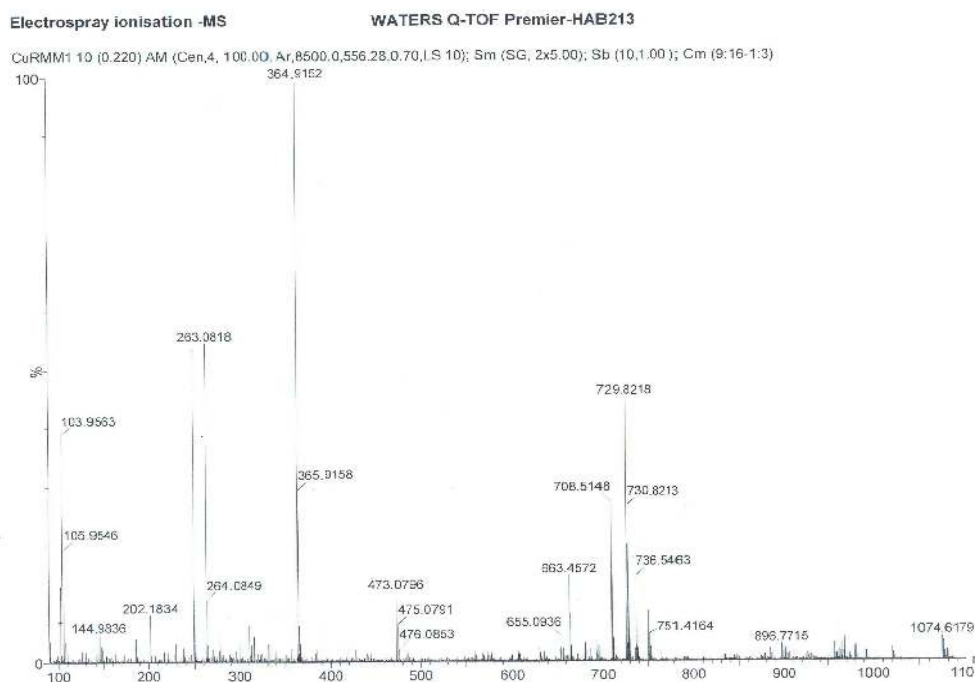


(a)



(b)

Supporting Information



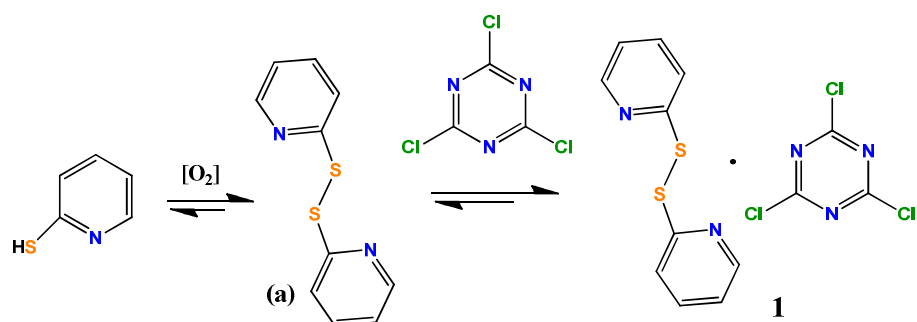
(c)

Fig. S3 ESI-MS spectra of (a) **1**, (b) **2** and (c) **4**

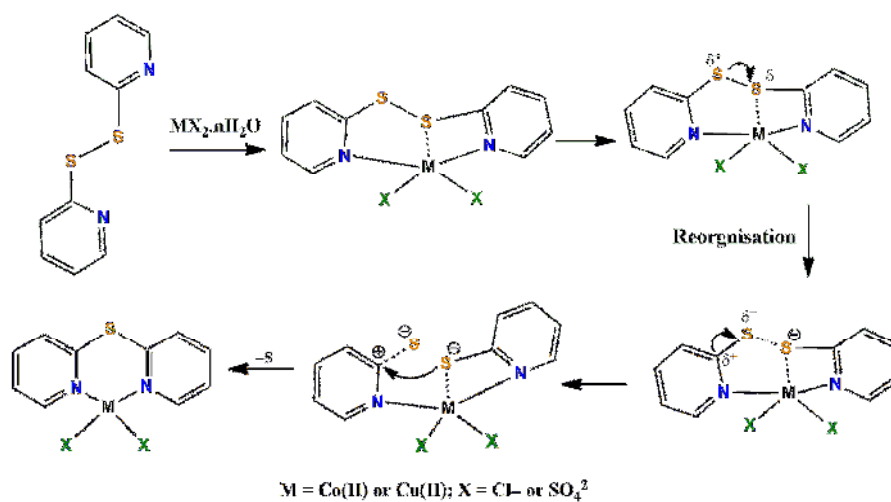
Mechanisms:

The mechanisms for disulfide bond formation has been proposed by various oxidative S-S coupling routes (Scheme S1).¹ Further, based on metal mediated thiolate/ sulphonate formation², we have proposed herein the plausible mechanism for desulfurization reaction (Scheme S2). The 2-PySSPy coordinates with the metal ion through both the nitrogen donor sites and also weakly interacts with one of sulphur atom to form four member chelate ring.³ Withdrawal of electron density from interacting sulfur atom makes it electron deficient relative to the other sulfur atom thereby pulling electron density from other sulfur atom. The other sulfur atom further withdraws electron density from adjacent carbon and creates partial positive charge on carbon atom. This step is followed by attack of sulfur atom (which is involved in the interaction with metal ion) on electron deficient carbon atom to form new C-S bond. It induced desulfurization of other sulfur atom to form **1'** that is coordinated to the metal centre.

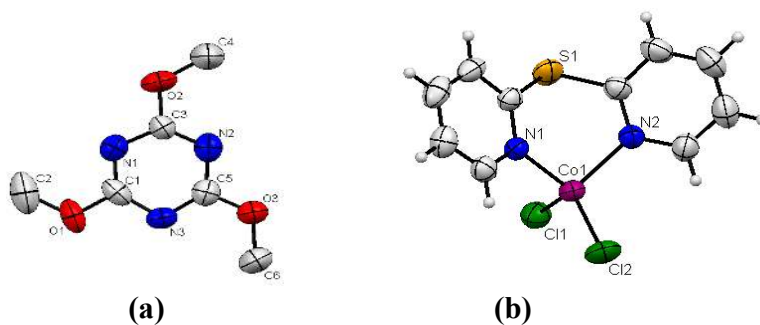
Supporting Information



Scheme S1 Plausible mechanism for the formation of co-crystal **1**.



Scheme S2 Plausible mechanism for the formation of **3** or **4** via metal mediated desulfurization reaction.



Supporting Information

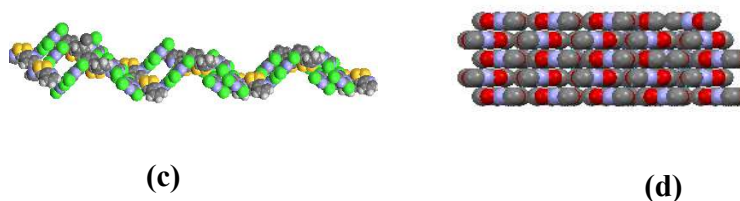


Fig. S4 Crystal structure of (a) **2** and (b) **3** with 30% ellipsoid probability. (c) Double helical structure of **1** generated through short contact interactions along crystallographic 'a'-axis; (b) Graphite type arrangement of **2** generated by short contact interactions along crystallographic 'a'/'c' axis.

X-ray crystallography and structure solution. Single crystal X-ray data for **1**, **2**, **3** and **4** were collected on a Rigaku R-Axis RAPID II diffractometer at room temperature using graphite-monochromated Mo-K α radiation ($\lambda = 0.71073$ Å). The crystallographic and refinement data for **1**, **2**, **3** and **4** are summarized in Table 1. Structures were solved by direct methods and refined by full-matrix least squares on F^2 (SHELXL 97, 2012).⁴ Non-hydrogen atoms were refined with anisotropic thermal parameters. All the hydrogen atoms were geometrically fixed and refined using a riding model. Computer program PLATON was used for analyzing the interaction and stacking distances.⁵ CCDC- 1505819 (**1**), 1505820 (**2**), 1505821 (**3**) and 1505822 (**4**) contain the supplementary crystallographic data for this paper. These data can be obtained free of charge *via* <http://www.ccdc.cam.ac.uk/conts/retrieving.html> (or from the CCDC, 12 Union Road, Cambridge CB21EZ, UK; Fax: +44-1223-336033; E-mail: deposit@ccdc.cam.ac.uk).

Crystal Structure of 1-4.

Eight units of cyanuric chloride and six units of 2-PySSPy complete the unit cell packing of **1**. (omitted for clarity). The pyridyl rings in 2-PySSPy oriented transoid to one another and involved in H \cdots bonding with cyanuric chloride which might be driving force for co-crystallization of cyanuric chloride with 2-PySSPy. The distance between 2-PySSPy and cyanuric chloride is 2.79 Å as calculated by shortest distance between N1 (2-PySSPy) and N2 (CC). The driving force for co-crystallization are weak interactions (N \cdots N, Cl \cdots N, C-H \cdots Cl and C-H \cdots π etc.). However, **1** does not involve any classical hydrogen bonding interactions due to absence of hydrogens at heteroatom. Likewise, it lacks $\pi\cdots\pi$ interactions too, owing to the loss of planarity by

Supporting Information

perpendicular arrangements of the pyridyl ring and cyanuric chloride ring with an inter-planar angle of 71.36° . The short contact interactions construct double helical arrangement in **1** as shown in Fig. S4(c). The S-S bond length in 2-PySSPy dimer is 2.03 \AA while other bond lengths are comparable to the known analogous systems [21-26 in the main text body)]. The S-S-C angle in 2-PySSPy is 104.27° whereas C-S-S-C torsion angle is -87.14° , indicated almost perpendicular arrangement of pyridyl rings of PySSPy moiety. In addition, synthesis and the crystal cell parameters of **2** are known previously (Table S1; Fig. S4a) [30 in the main text body] Most interesting feature of **2** is graphite type layer constructed through short contact interactions along all the axes especially 'a' and 'c' crystallographic axes (Fig. S4d).

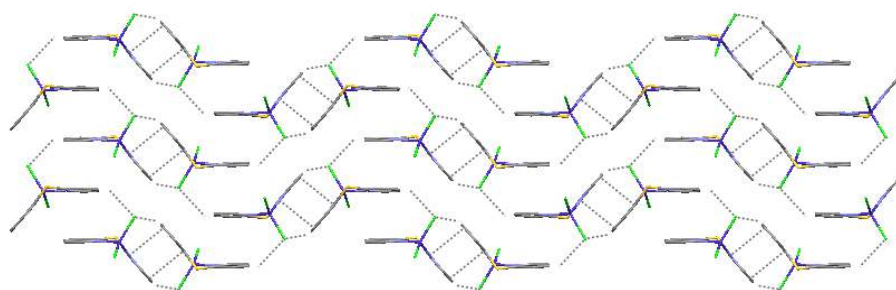
Saturated MeOH solution of **3** yielded block shaped crystals suitable for single crystal X-ray analysis. Complex **3** crystallizes in monoclinic crystal system with P21/c space group (Table S1). The asymmetric unit contains its complete structure comprising one molecule of **1'** and Co(II) along with two chloride units (Fig. S4b). The Co(II) centre assumes distorted T_d geometry which is completed by N,N donor sites of **1'** and two Cl^- ligands. Ligand **1'** becomes quite non-planar in coordinated mode that can be estimated by its pyridyl rings mutually orientated by angle of 50.11° . The structure exhibits good symmetry which is reflected by the Cl-Co-Cl plane that divides **1'** into two equal parts. Likewise, N-Co-N plane also divides both the chlorines equally along with the pyridyl rings of **1'** into two equal halves (however sulfur atom remains at one end of plane). The six member chelate ring lies in the non planar fashion wherein Co(II) and 'S' atoms are tilted at one side and rest four pyridyl ring carbon atoms are tilted at the opposite end. The N1-Co-N2 bite angle is smallest (95.26°) whereas the largest bite angle Cl(1)-Co-Cl(2) is (116.31°) that shows the extent of distortion from ideal T_d geometry (Fig. S4b). The Co-N and Co-Cl bond lengths are almost equal and found to be $\sim 2.034 \text{ \AA}$ and $\sim 2.232 \text{ \AA}$, respectively [21-26-27b in the main text body]. The $\pi \cdots \pi$ interactions through one of the pyridyl rings resulted in the formation of dimeric structure in *anti*-fashion with a centroid-centroid distance of 3.64 \AA . The intra- and inter-molecular $\text{H} \cdots$ bonding interactions are absent in **3**. The short contact interactions lead to the construction of 2D-ladder architecture along 'c' crystallographic axis (Fig. S5a).

Supporting Information

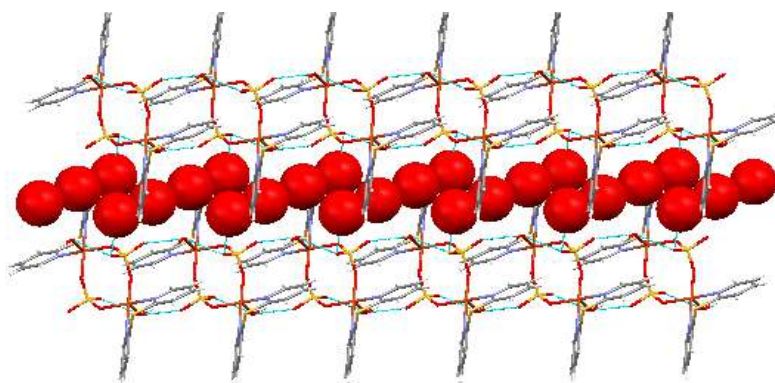
The re-crystallization in MeOH/MeCN media afforded block shaped single crystals of **4**. Complex **4** crystallized in triclinic crystal system with $P\bar{1}$ space group (Table S1). Crystallographic analysis revealed dimeric structure of **4** comprising two units of each; Cu(II), **1'**, SO_4^{2-} , coordinated H_2O and lattice H_2O (Fig. 1b, main text body). However, asymmetric unit encompasses half of the dimeric structure having one unit of each of Cu(II), **1'**, SO_4^{2-} , coordinated H_2O and notably both the lattice H_2O molecules. The Cu(II) centers assume distorted square pyramidal (SPy) geometry completed by N,N-donor site of **1'**, two oxygens of two sulphate ligands and a coordinated water molecule. The bite angles about Cu(II) centers suggest almost ideal SPy coordination environment wherein the basal square plane is occupied by two nitrogen atoms and two sulphate oxygen atoms and the apical position is occupied by coordinated water molecule. The Cu(II)···Cu(II) distance in **4** is 4.93 Å which may play significant role in the magnetic behavior. However, the complex is dimeric and therefore magnetic behavior might be ordinary [31 in the main text body] though it is a subject of investigation in magnetic properties based work in future [31 in the main text body]. Moreover, sulphate ligands maintain almost regular T_d geometry despite in μ -sulphato coordination mode (Fig. 1b, main text body). Ligand **1'** assumes non planar orientation in **4** too, with interplanar pyridyl-pyridyl ring angle of 62.20° which is relatively larger than that for **3**. It may be ascribed to the SPy geometry (62.20°) in **4** over T_d geometry (50.11°) in **3**.

The Cu-N bond lengths are ~2.006 Å which is shorter than that of Co-N bond distances (~2.034 Å) whereas Cu-O bond lengths are approximately equal (~1.948 Å) [20-27-32]. The cavity created by sulphate ligands, Cu(II) and coordinated H_2O having size dimensions ~3.17 × 4.93 × 5.35 Å which can be suited to accommodate guest molecule (*vide supra*). It entails intramolecular H···bonding interactions between O5-H5···O3 atoms and these O5 and O3 atoms are also involved in intermolecular H···bonding interactions with O2 and O7 atoms (O5-H5···O2; O7-H7···O3). The combined contributions of intra- and intermolecular H···bonding interactions construct infinite 2D network with a *zig-zag* water channel shown along crystallographic 'c'-axis (Fig. S5b). Notably, $\pi\cdots\pi$ and C-H··· π interactions are absent in **4**.

Supporting Information

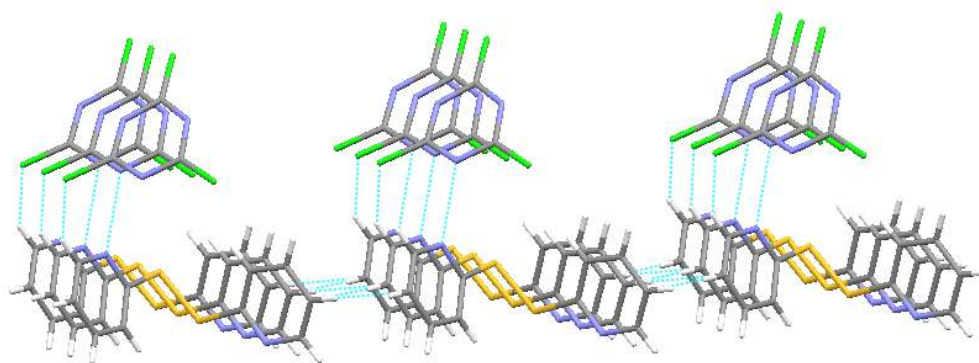


(a)



(b)

Fig. S5 (a) 2D-ladder architecture *via* short contact interactions in **3**; (b) 2D water channel network *via* H \cdots O bonding interactions in **4**



(a)

Supporting Information

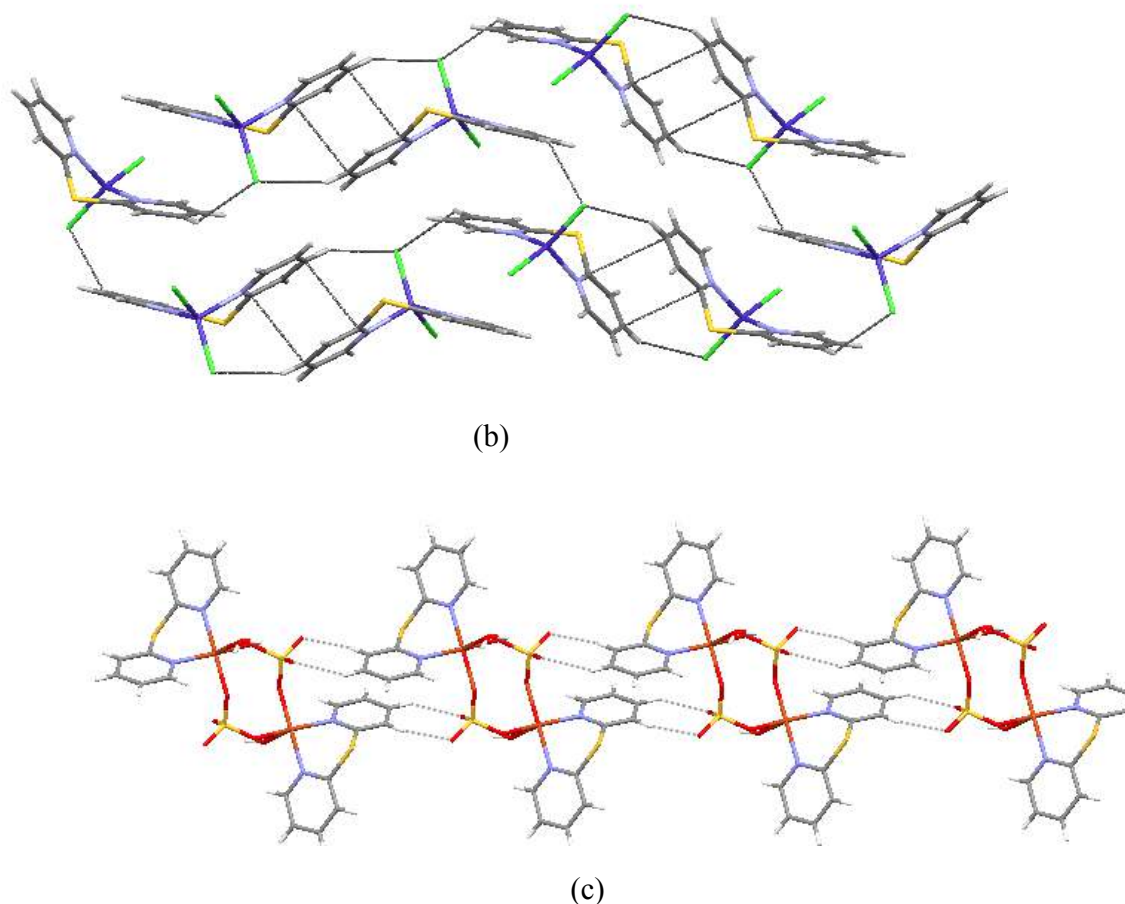


Fig. S6 Intermolecular interactions in **1** (a), **3** (b) and **5** (c) that may result J-aggregation

Electronic spectroscopy: UV/vis and fluorescence. The UV/vis spectra of **1-4** displayed prominent bands between 215 to 350 nm in H₂O (Fig. S7a). Compound **1** exhibited three bands at 280 nm (ϵ , 53,963 M⁻¹cm⁻¹), 232 nm (ϵ , 67,542 M⁻¹cm⁻¹) and 210 nm (ϵ , 67,860 M⁻¹cm⁻¹) assignable to the n- π^* and π - π^* transitions in **1**. Conversely, **2** displayed only a weak hump at 239 nm (ϵ , 11,001 M⁻¹cm⁻¹) and a strong π - π^* transition at 208 nm (ϵ , 85,052 M⁻¹cm⁻¹). Complex **3** displayed low energy (LE) band at 280 nm (ϵ , 32,839 M⁻¹cm⁻¹) and high energy (HE) band at 234 nm (ϵ , 44,711 M⁻¹cm⁻¹) which is closely matching to the two lower energy bands in **1**. Notably, the binuclear Cu(II) complex **4** displayed LE band at 282 nm (ϵ , 74,808 M⁻¹cm⁻¹) and strong HE band at 232 nm (ϵ , 1,11,497 M⁻¹cm⁻¹). The HE band is red shifted relative to the both **1** and **3** due to the formation of sulphato bridged dimeric complex **4**.

Supporting Information

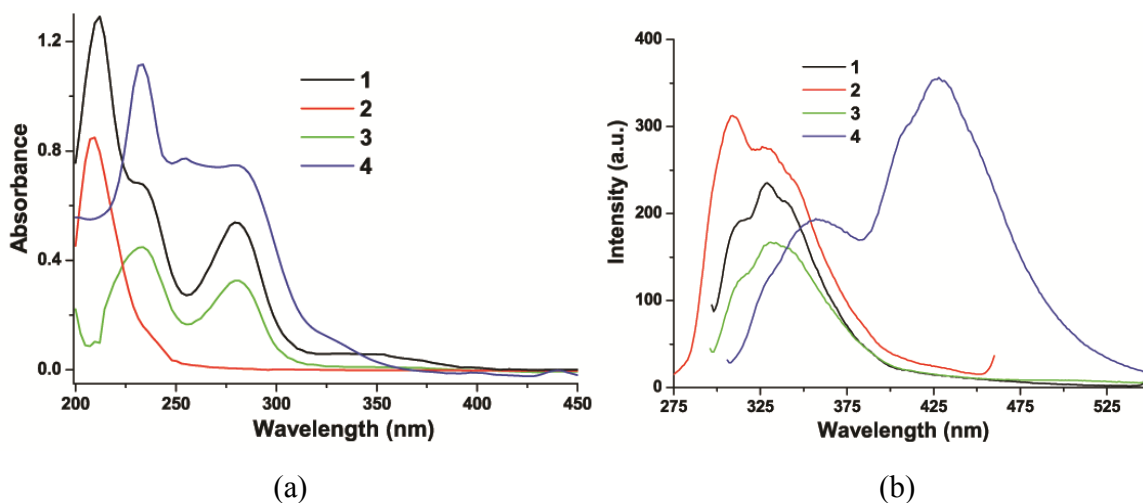


Fig. S7. UV/vis (a) and fluorescence (b) spectra of **1-4** in H₂O.

Upon excitation (λ_{ex}) at 280 nm, **1** exhibited moderate emission at 328 nm with quantum yield (ϕ_{fl}) determined to be 0.37 and Stokes shift (SS) of 5226 cm⁻¹ (Fig. S7b). Highly planar molecule **2** showed stronger emission at 308 nm (ϕ_{fl} , 0.58; SS, 9906 cm⁻¹) upon excitation at 236 nm. The fluorescence intensity of **3** is slightly better to that of **1** as evident from its quantum yield (ϕ_{fl} 0.43; SS, 5594 cm⁻¹), however, the wavelength of emission maxima (λ_{max}) remains unchanged. Although, **1-3** exhibited emission with almost overlapped dual bands probably due to the intermolecular aggregations (Fig. S4d & Fig. S6) but **4** exhibited rather distinct dual emissions having maxima at 355 (SS, 6314 cm⁻¹) and 427 nm (SS, 11064 cm⁻¹). The LE band is more intense than that of the HE band and the ϕ_{fl} for **4** determined to be 0.60. The fluorescence quenching in Cu(II)-complexes is well known and therefore fluorescent Cu(II)-complexes particularly with high quantum yield are of special interest and importance.[32 in the main text body] In **4**, both the emission band maxima lie at higher wavelength than those of **1-3**. The cause of dual emission in **4** was assumed to be associated with the formation of intermolecular aggregates. To have a deep insight into this assumption, we further analyzed single crystal X-ray data of **1**, **3** and **4** and found that all of these can form intermolecular J-aggregation but extent can be different (Fig. S6). To verify it, the solution of **4** was further diluted (10⁻⁵ M to 10⁻⁷ M) which led to the increase in intensity of HE band and decrease in the LE band (Fig. S8). It clearly suggests that the LE intense band is associated with the intermolecular J-aggregation.

Supporting Information

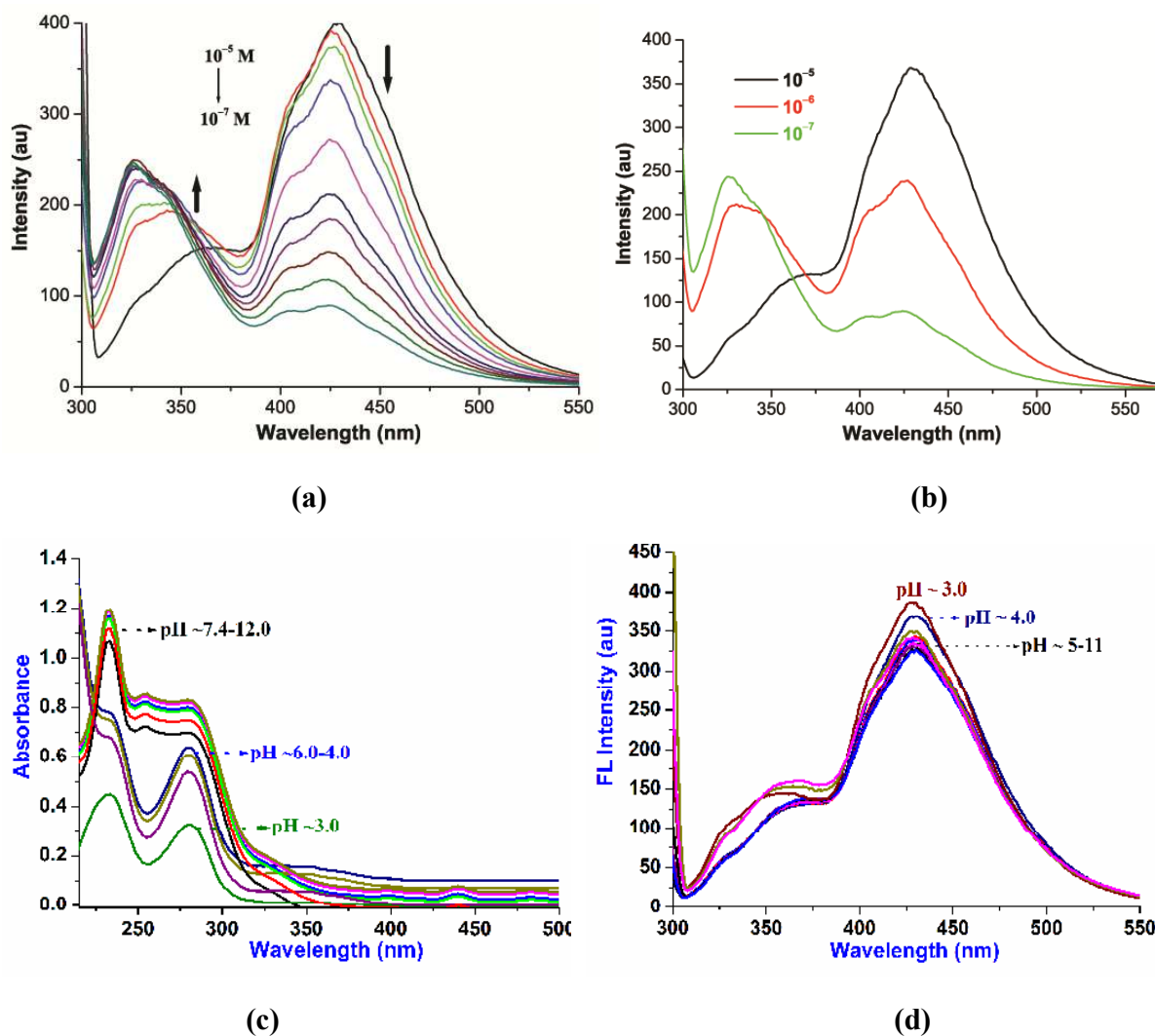


Fig. S8 Fluorescence spectra of **4** by diluting solution to check J-aggregation in buffer/H₂O solution (1.0 M Tris-HCl pH = 7.4) (a, b); UV/vis (c) and Fluorescence (d) spectra of **4** at basic to acidic pH range in H₂O.

Supporting Information

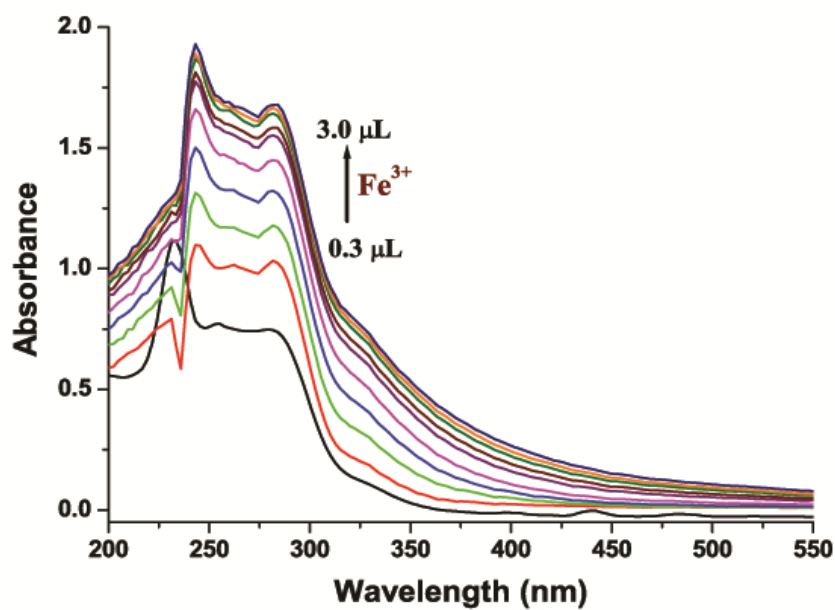


Fig. S9 UV/vis titration plot for **4** with Fe^{3+} ion in buffer/ H_2O solution (1.0 M Tris-HCl pH = 7.4).

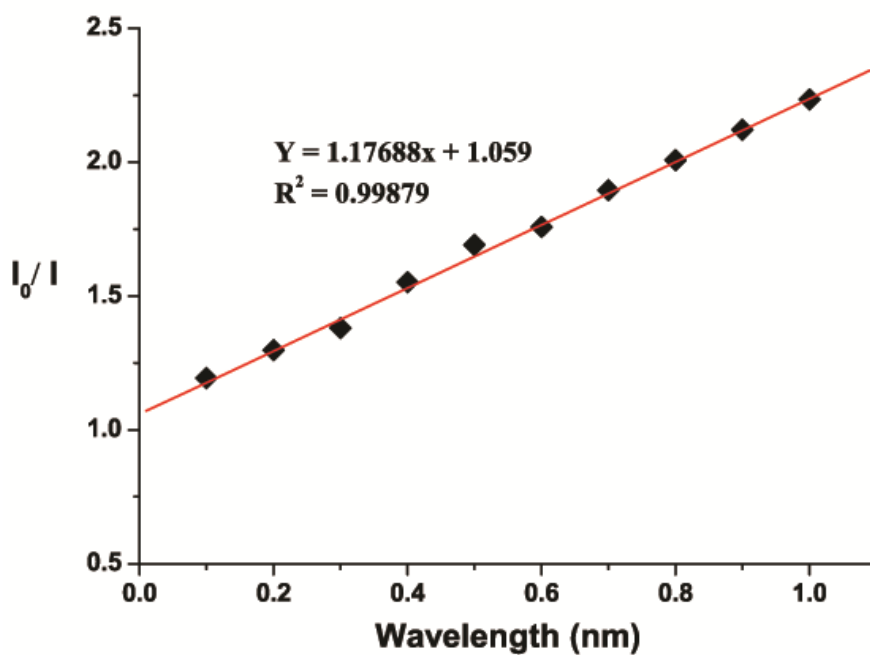


Fig. S10 Stern-Volmer plot for **4** and Fe^{3+} ion

Supporting Information

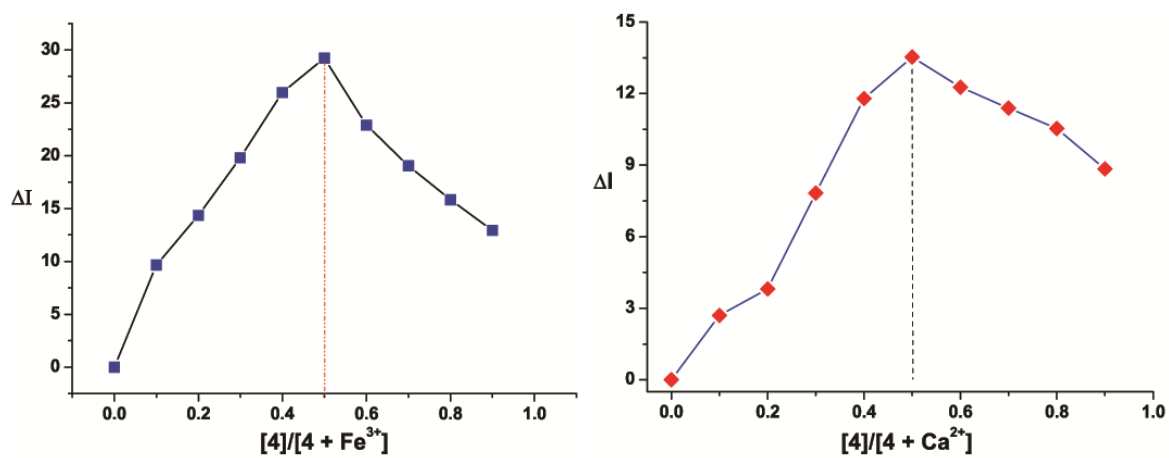


Fig. S11 Jobs plot analysis for $4+\text{Fe}^{3+}$ ion $4+\text{Ca}^{2+}$ ion

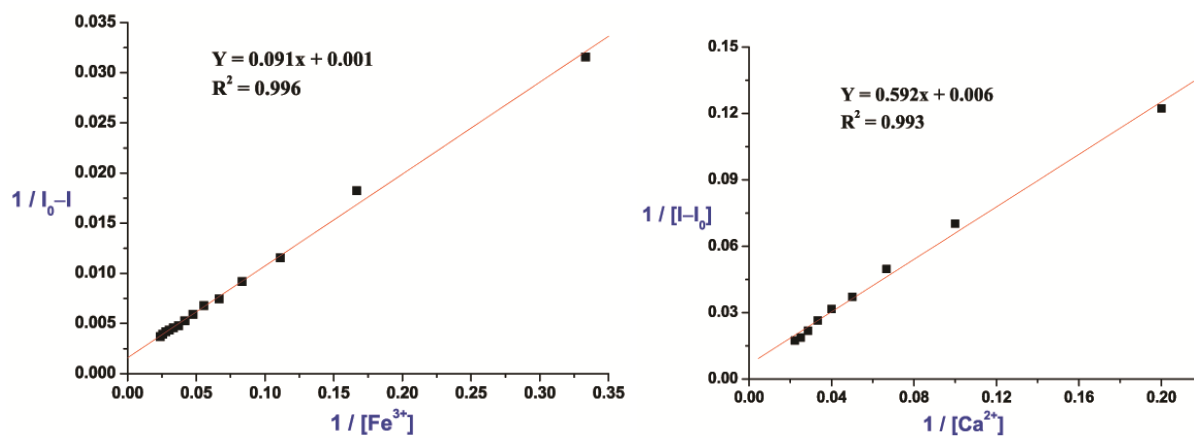


Fig. S12 Benesi-Hildebrand plot for $4+\text{Fe}^{3+}$ ion $4+\text{Ca}^{2+}$ ion

Supporting Information

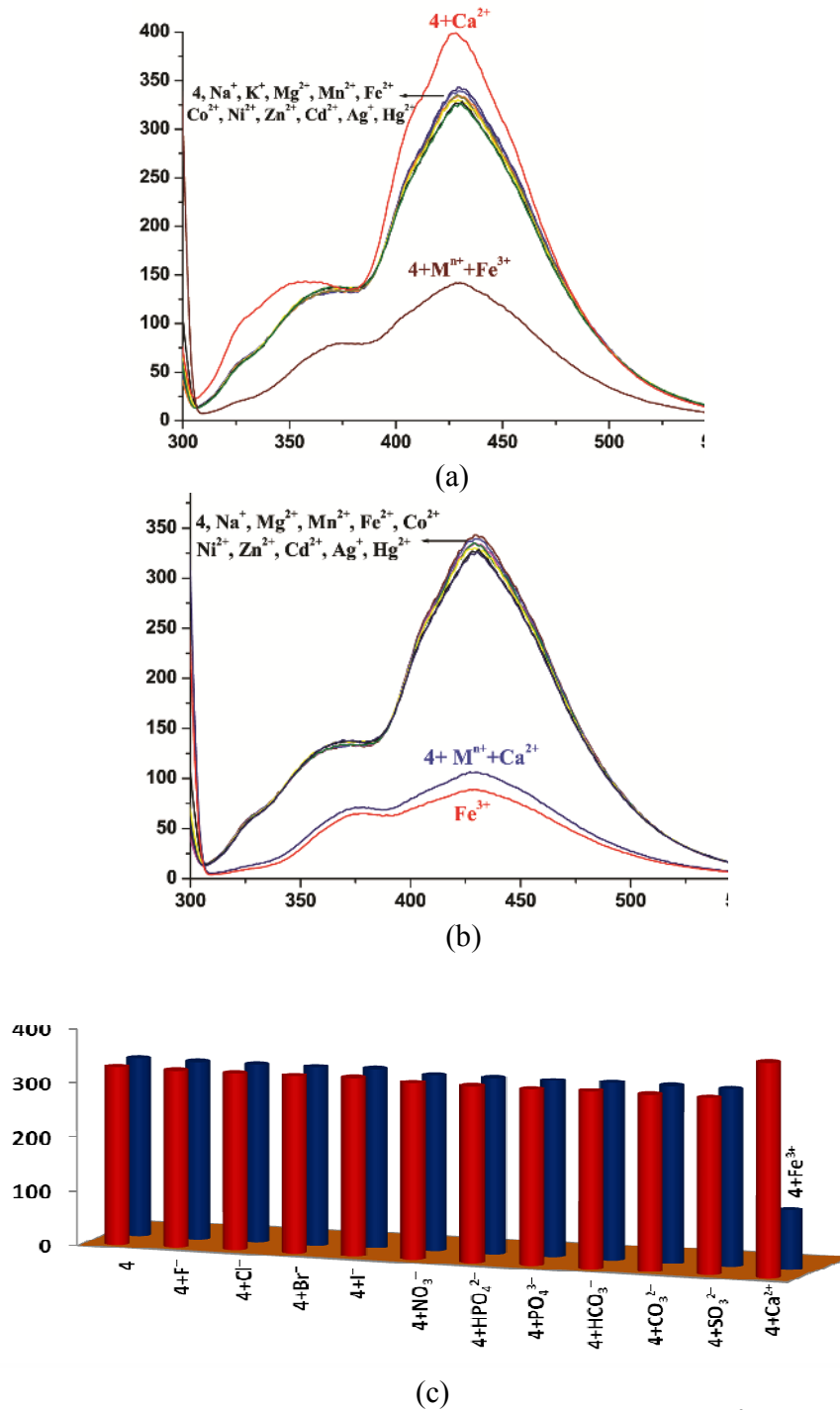


Fig. S13 Interference of various metal ions to the plot for (a) $4+Fe^{3+}$ complex (b) $4+Ca^{2+}$ complex and (c) Interference of various anions to $4+Ca^{2+}$ and $4+Fe^{3+}$ complex.

Supporting Information

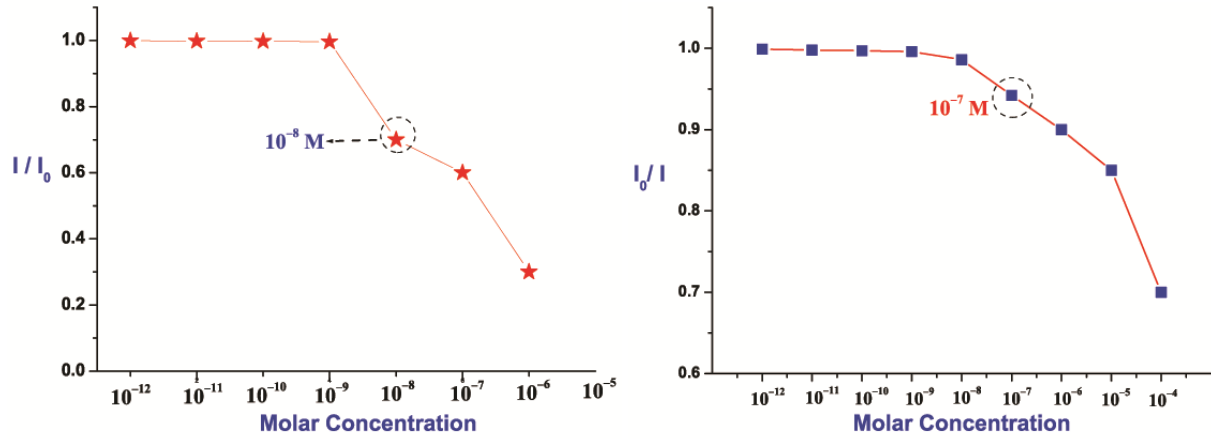


Fig. S14 Fluorescence sensitivity of **4** for Fe^{3+} (left) and Ca^{2+} (right) ions

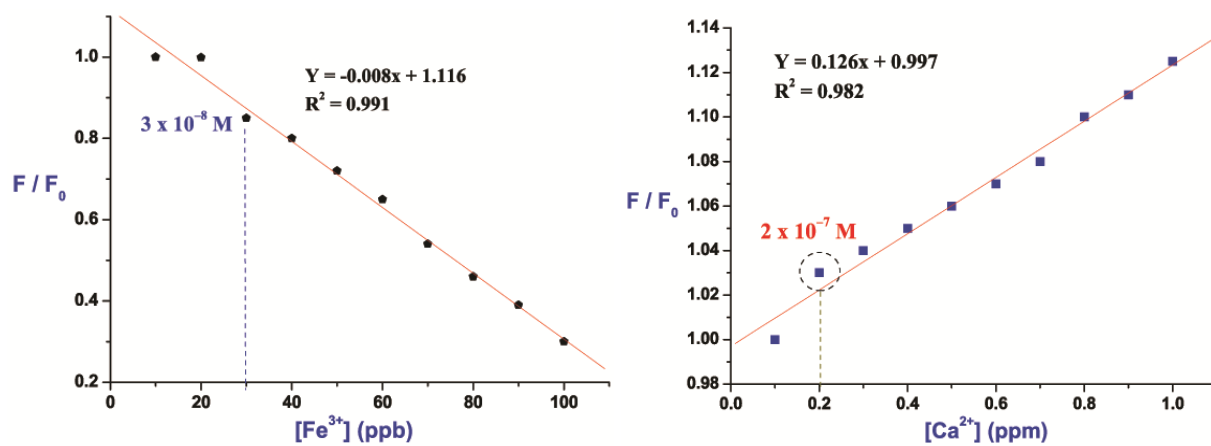
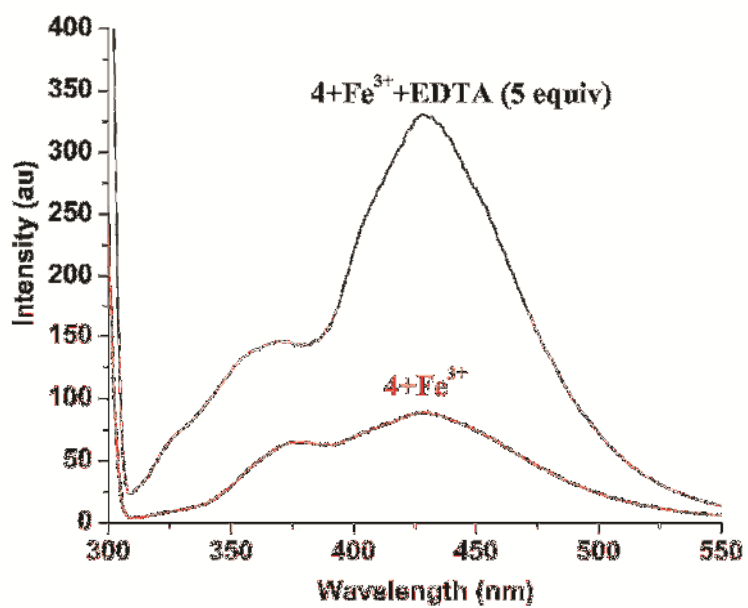
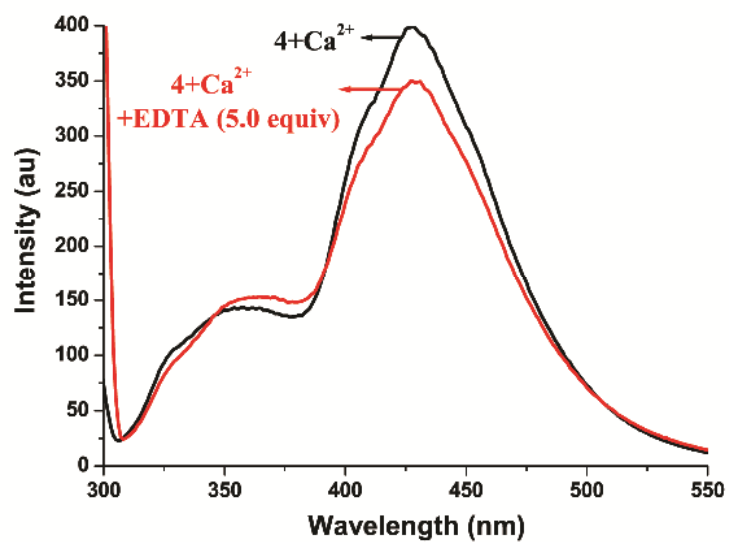


Fig. S15 Fluorescence LOD of **4** in presence toward (a) Fe^{3+} and (b) Ca^{2+} ions

Supporting Information



(a)



(b)

Fig. S16 Reusability of **4** for the detection of (a) Fe³⁺ and (b) Ca²⁺ ions using EDTA

Supporting Information

Discussion on Binding Site for Fe³⁺/Ca²⁺.

The positive response of **4** toward Fe³⁺/Ca²⁺ ions and insignificant response toward sulphurphilic metals Cu²⁺, Cd²⁺, Hg²⁺, Pb²⁺ etc. indicated the interaction site other than 'S'-atom(s) of **4**. To have deep insight, we acutely examined the structure of **4** from X-ray single crystal data which suggests six oxygen atoms of dimeric **4** as a quite possible interaction site for Fe³⁺ and Ca²⁺. As a matter of fact, four oxygens from two bridged sulphate groups (O1 and O3 of dimeric **4**) and two oxygen atoms from coordinated water molecules (O5 of dimeric **4**) create an environment similar to the six coordination site offered by pseudo-crown-6 ether system for cations to assume octahedral (O_h) geometry (Fig. S17). For better understanding, we added created a centroid among all six oxygen atoms and assumed it as a cation. Notably, the bond distance between four sulphate oxygen atoms and centroid are found in the range ~ 2.38-2.12 Å while bond distances between two water oxygen and centroid bond are relatively long (3.45 Å) (Fig. S17). It further strengthened our postulation that Fe³⁺ and Ca²⁺ may assume distorted O_h geometry or rhombic geometry (Fig. 7) occupied by six oxygen atoms (O1, O3 and O5 of dimeric **4**). Both Ca²⁺ (ionic radius, ~1.08 Å) and Fe³⁺ (~0.57-0.68 Å) can fit well within six oxygen atoms of **4**. It is evident by measuring the distance between anti-disposed oxygen atoms [O1···O1 (4.24 Å), O3···O3 (4.76 Å) and O5···O5 (6.89 Å)] of **4** interacting with Ca²⁺ and Fe³⁺. Rationally, it is further affirmed by measuring the actual distances between anti-disposed N···O atoms (N₂O₂ donor set) coordinated to Cu(II) centers in **4** which are having smaller distances [N2···O1 (3.92 Å) and N1···O4 (3.95 Å)]. Moreover, the proposed binding mode supports 1:1 binding mode suggested by Job's plot analysis. Notably, despite several attempts, we could not get single crystals of **4**·Fe³⁺ and **4**·Ca²⁺ complexes. In addition, EPR study also suggested rhombic symmetry of HS Fe(III) ion which corroborates well with the three unequal distances in **4**·Fe³⁺ (*vide supra*).

To get better insight, the Co(II)-complex **3** that comprises same ligand (but does not entail sulphato bridged dimeric structure like **4**) was used as a model probe for metal ions (Scheme 2 and Fig. S4b). To our delight, none of the metal ion (10.0 equiv) could induce considerable change in the fluorescence spectral feature of **3** (Fig. S18). It strongly supported our proposed interaction site of **4** toward Fe³⁺ and Ca²⁺ ions. The binding of crown ethers with Fe³⁺ and Ca²⁺ ions is well known³⁵ which further strengthens the possibility of interaction of doubly bonded

Supporting Information

oxygens with these cations in our system. The binding site of metalloreceptor **4** is although not a pseudo-crown ether moiety but its nature (doubly bonded oxygen atoms) and orientation resemble with pseudo-crown ethers.

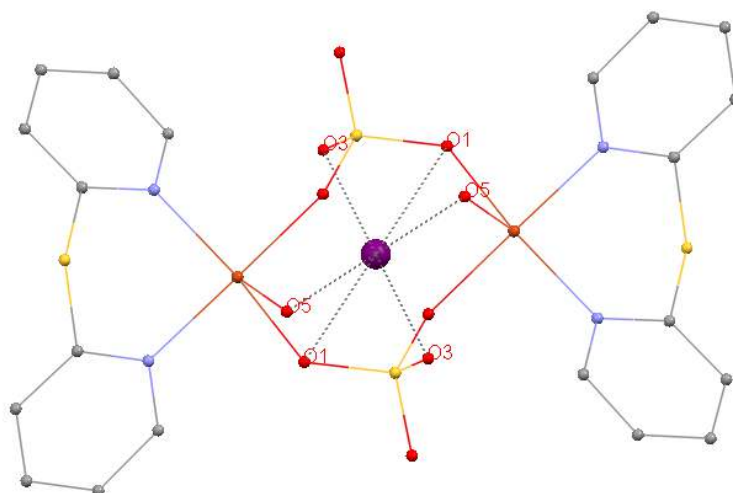


Fig. S17. Plausible interaction modes of **4** with Fe^{3+} and Ca^{2+} ions (purple sphere assumed to be $\text{Fe}^{3+}/\text{Ca}^{2+}$). This model is artificially created from single crystal data of **4** thereafter adding centroid amongst six oxygen atoms as possible interaction site.

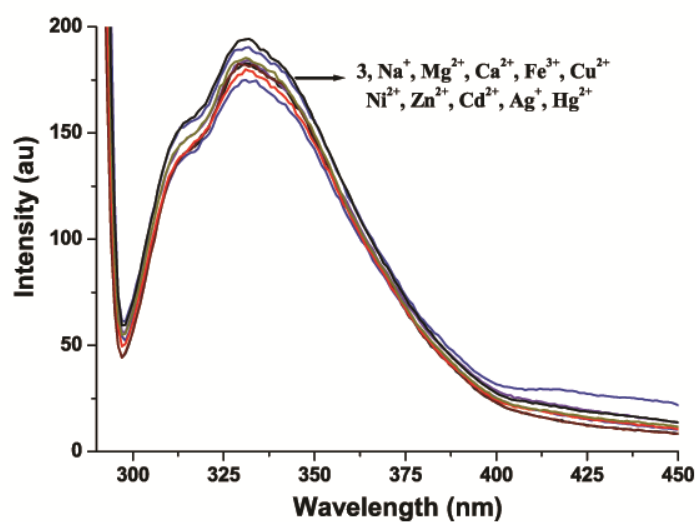
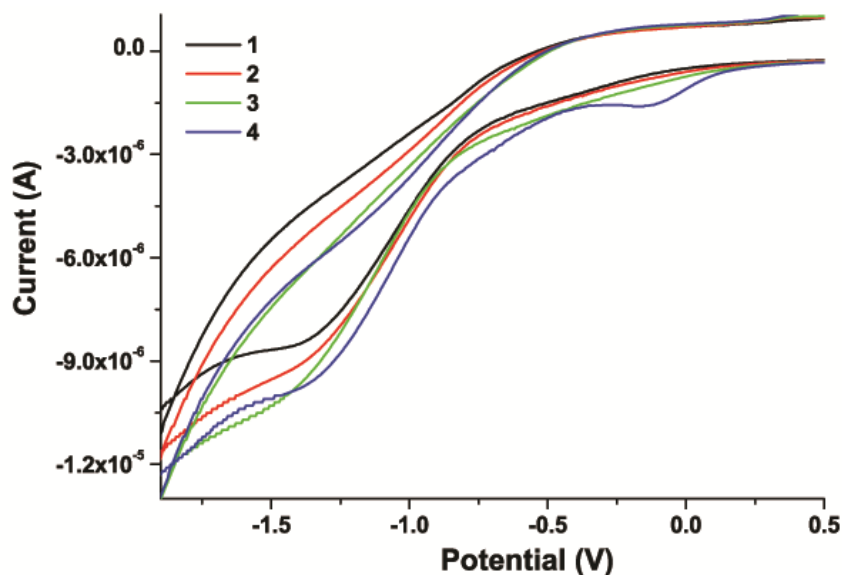


Fig. S18 Fluorescence spectrum of **3** in presence of various metal ions

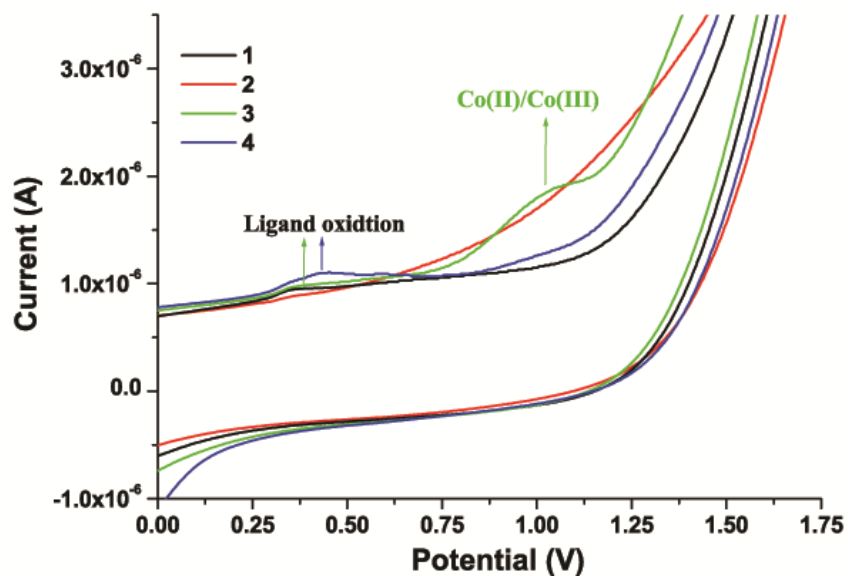
Supporting Information

Electrochemical studies. The redox behavior of **1-4** was investigated by cyclic voltammetry in the potential range -2.0 to $+2.0$ (Fig. S19). The cyclic voltammogram of **1** exhibits an irreversible single reductive wave -1.36 V and a single oxidative wave at 0.37 V at a scan rate of 0.1 V/s. The reductive wave may be attributed to the reduction of pyridyl ring nitrogens whereas oxidative wave may be associated with the oxidation of sulfur atom. Further, **2** displays a poorly defined irreversible single reductive wave at -1.39 V probably due to the cyanuric ring nitrogen reductions, while it does not show any oxidative wave. The Co(II) complex **3** exhibits an inadequately structured irreversible reductive wave at -1.42 V and markedly irreversible double oxidative waves at 0.38 V and 1.02 V. The earlier is associated with the ligand centered oxidation and the later is ascribed to the $\text{Co}^{2+}/\text{Co}^{3+}$ redox couple. Remarkably, Cu(II) complex **4** displays irreversible double reduction waves at -0.12 V and -1.36 V. The previous is ascribed to the $\text{Cu}^{2+}/\text{Cu}^+$ redox couple and the latter may be associated to the ligand centered reduction. In the anodic window, **4** shows a single oxidative wave at 0.45 V attributable to the ligand centered oxidation.



(a)

Supporting Information



(b)

Fig. S19 CV plots of 1-4 in reduction (a), oxidation (b) window

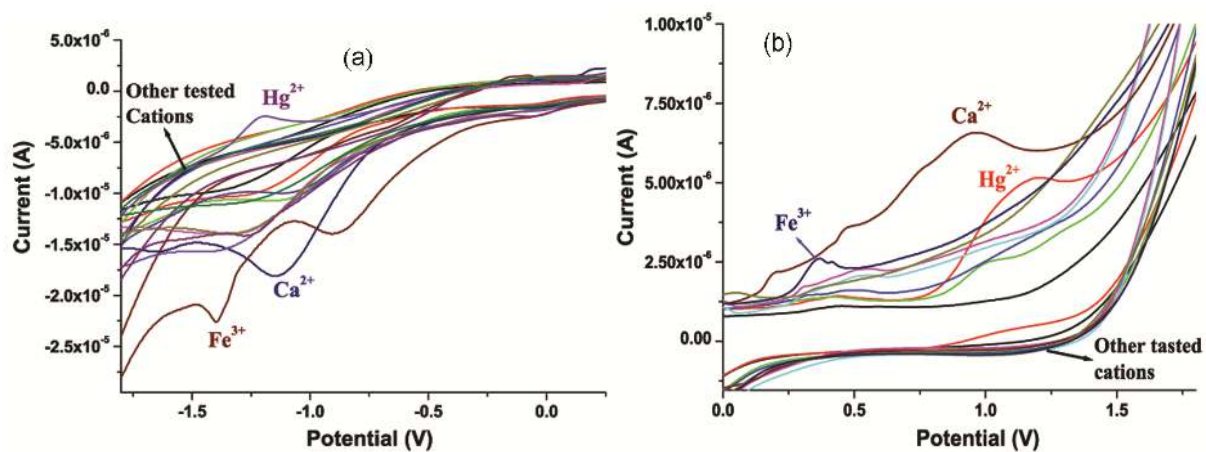


Fig. S20. Cyclic voltammogram of 4 in presence of 10.0 equiv of various metal ions, in reduction (left) and oxidation (right) window (H₂O/EtOH, 9:1, v/v).

Supporting Information

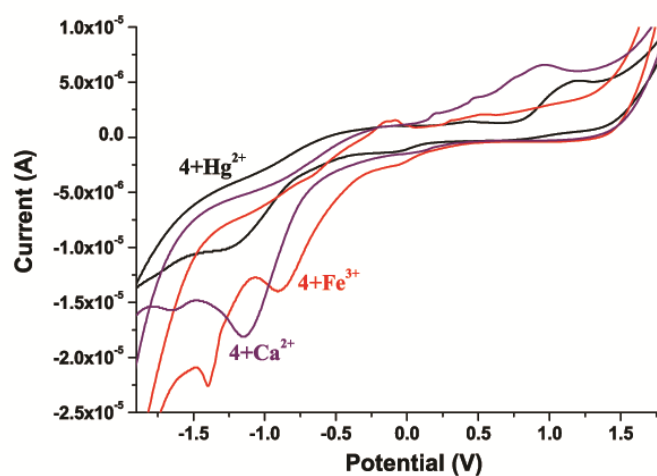
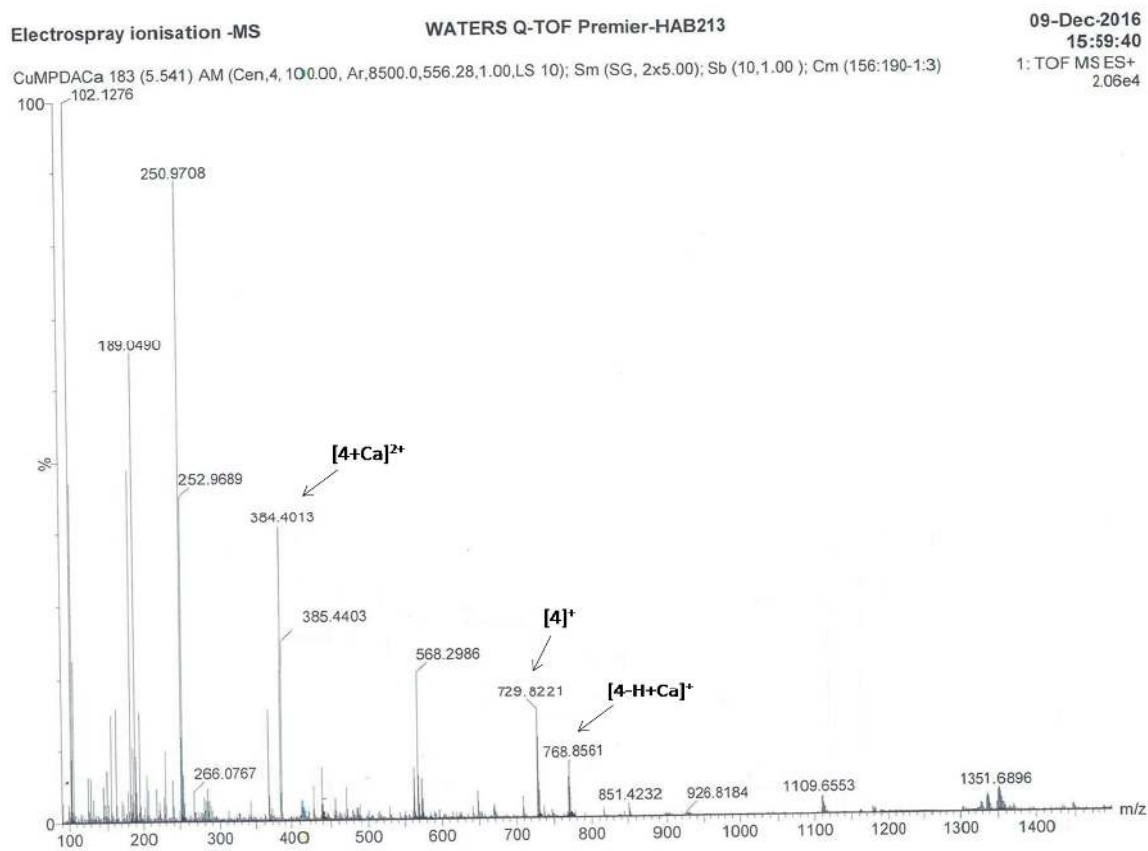
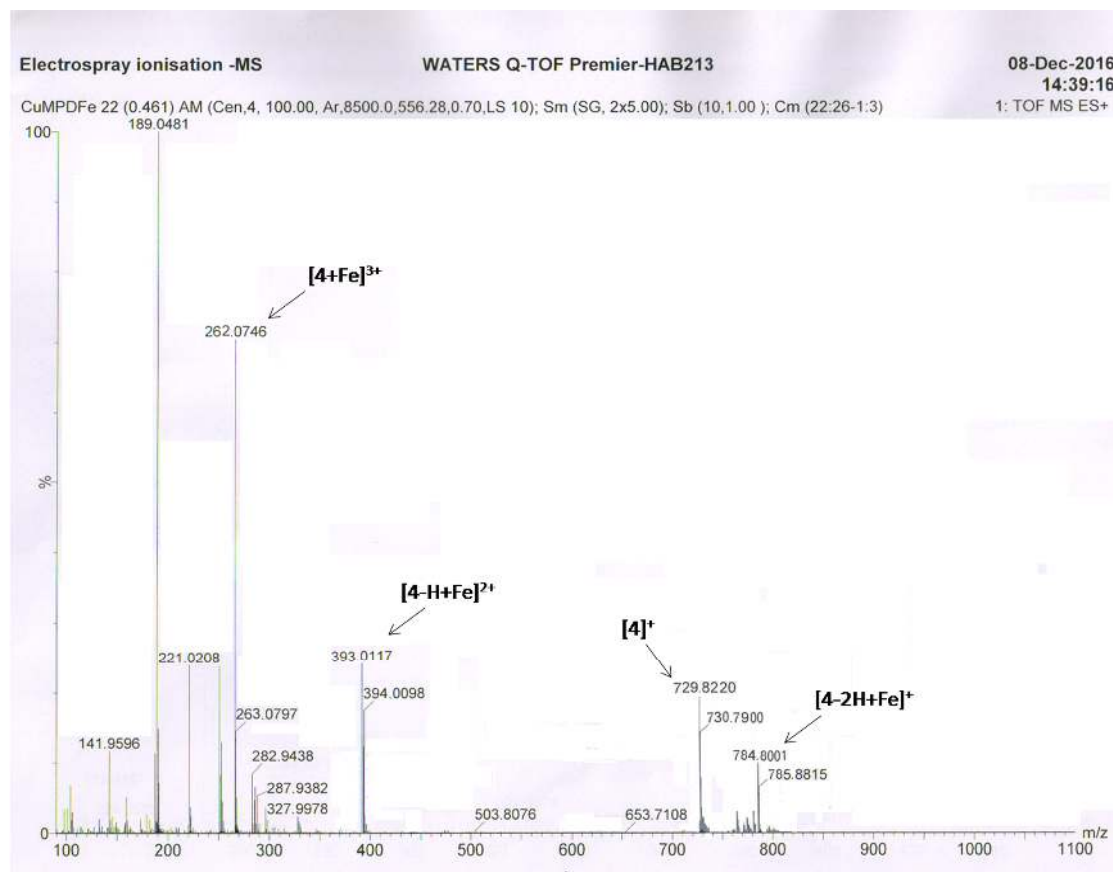


Fig. S21 Electrochemical interference of Hg^{2+} ion with $4+\text{Fe}^{3+}$ and $4+\text{Ca}^{2+}$ complexes.



(a)

Supporting Information



(b)

Fig. S22 ESI-MS spectra of $4+Ca^{2+}$ and $4+Fe^{3+}$ complexes.

Supporting Information

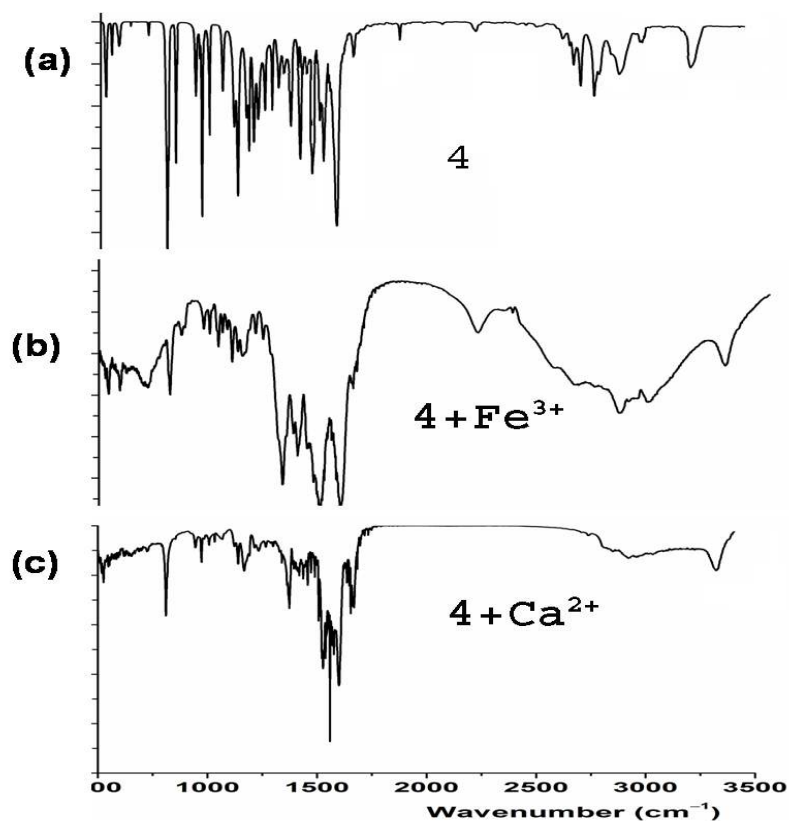


Fig. S23 FTIR spectra of 4 (top), 4+ Fe^{3+} (middle) and 4+ Ca^{2+} (bottom).

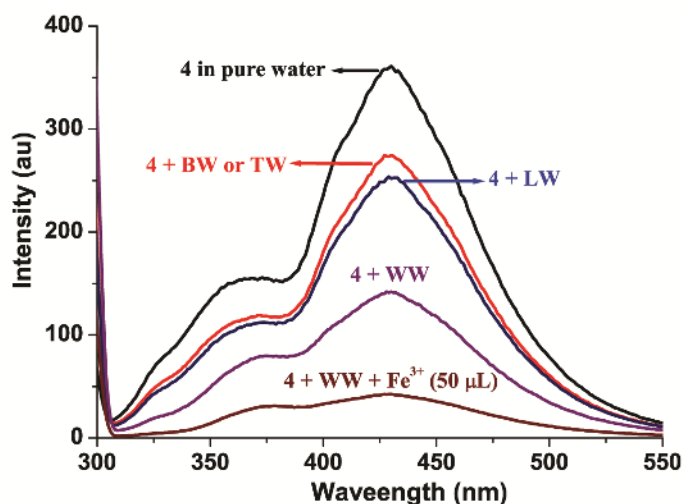


Fig. S24 Fluorescence quenching of 4 in various real water samples following order $\text{WW} > \text{LW} > \text{TW/DW} \approx$. (WW = Waste Water; LW = Lake Water; TW/DW = Tap/Drinking Water; BW = Bore well Water).

Supporting Information

Table S1. Crystallographic Parameters for **1-4**

Parameters	1	2	3	4
Empirical formula	C ₁₃ H ₈ Cl ₃ N ₅ S ₂	C ₆ H ₁₁ N ₃ O ₃	C ₁₀ H ₈ Cl ₂ CoN ₂ S	C ₂₀ H ₂₀ Cu ₂ O ₁₀ N ₄ S ₄
FW	404.72	173.18	318.07	731.74
Cryst. syst.	Monoclinic	Orthorhombic	Monoclinic	Triclinic
Space group	<i>C</i> 2/ <i>c</i>	<i>Pnma</i>	<i>P</i> 21/ <i>c</i>	<i>P</i> -1
a(Å)	20.900(4)	8.442(4)	12.289(3)	7.2021(13)
b(Å)	4.961(10)	6.7270(13)	7.6775(15)	9.469(3)
c(Å)	24.079(5)	14.467(3)	14.314(3)	11.699(3)
α(°)	90	90	90	66.533(13)
β(°)	102.14(3)	90.00	110.80(3)	80.57(3)
γ(°)	90	90	90	81.58(3)
Volume (Å ³)	2441.0 (9)	821.6(5)	1262.5(5)	719.0(3)
Color and habit	Light Yellow, block	White, block	Pink, block	Blue, block
Z	4	4	4	2
Density calcd. (gcm ⁻³)	1.603	1.400	1.673	1.856
Abs. coeff. (mm ⁻¹)	0.898	0.113	1.919	1.845
<i>F</i> (000)	1180.79	368	639.212	410
Crystal size (mm ³)	0.5×0.4×0.3	0.3×0.2×0.1	0.6×0.5×0.4	0.6×0.4×0.2
θ range (deg)	3.46 to 27.48	3.34 to 25.00	3.04 to 27.43	2.11 to 28.20
Reflns collected	11384	5749	11774	340
Ind. Reflns	1595	521	2401	2042
	[<i>R</i> _{int} = 0.121]	[<i>R</i> _{int} = 0.167]	[<i>R</i> _{int} = 0.036]	[<i>R</i> _{int} = 0.0716]
reflns/restraint/ parameters	2795/0/144	785/0/76	2865/0/144	2440/0/199
Goodness-of-fit on <i>F</i> ²	1.017	1.776	0.873	1.042
Final <i>R</i> ind [<i>I</i> > 2σ(<i>I</i>)]	R1= 0.0728	R1= 0.1516	R1= 0.0286	R1= 0.0627
	wR2 = 0.243	wR2 = 0.434	wR2 = 0.113	wR2 = 0.174

Supporting Information

References:

- 1 (a) B. Mandal, B. Basu, *RSC Adv.* 2014, **4**, 13854-13881; (b) R. Hunter, M. Caira, N. Stellenboom, *J. Org. Chem.* 2006, **71**, 8268-8271; (c) M. Bao, M. Shimizu, *Tetrahedron*, 2003, **59**, 9655-9659; (d) A. Khazaei, M. A. Zolfigol, A. Rostami, *Synthesis*, 2004, 2959-2961.
- 2 (a) L. F. Ma, Y. Y. Wang, L. Y. Wang, D. H. Lu, S. R. Batten, J. G. Wang, *Cryst. Growth Des.* 2009, **9**, 2036-2038; (b) L. F. Ma, L. Y. Wang, M. Du, *Cryst. Eng. Comm.* 2009, **11**, 2593-2596; (c) S. Delgado, A. Barrilero, A. Molina-Ontoria, M. E. Medina, C. J. Pastor, R. Jiménez-Aparicio, J. L. Priego, *Eur. J. Inorg. Chem.* 2006, 2746-2759; (d) A. I. Gallego, O. Castillo, F. Zamora, S. Delgado, *RSC Adv.* 2013, **3**, 18406-18413.
- 3 S. D. Dwivedi, S. K. Dubey, A. K. Singh, K. K. Pandey, D. S. Pandey, *Inorg. Chim. Acta.* 2010, **363**, 2095-2103.
- 4 (a) G. M. Sheldrick, *SHELXL-97*, Program for X-ray Crystal Structure Refinement; Göttingen University: Göttingen, Germany, 1997; (b) G. M. Sheldrick, *HELXS-97*, Program for X-ray Crystal Structure Solution; Göttingen University: Göttingen, Germany, 1997.
- 5 (a) A. L. Spek, *PLATON*, A Multipurpose Crystallographic Tools Utrecht University, Utrecht, The Netherlands, 2000; (b) A. L. Spek, *Acta Crystallogr. A* 46 (1990) C31.